Bioresource Technology 130 (2013) 144–151

Contents lists available at SciVerse ScienceDirect

Bioresource Technology

journal homepage: www.elsevier.com/locate/biortech

Analysis of metabolic fluxes for better understanding of mechanisms related to lipid accumulation in oleaginous yeast *Trichosporon cutaneum*

Zhijie Liu [a], Yang Gao [a], Jun Chen [a], Tadayuki Imanaka [a,b], Jie Bao [a], Qiang Hua [a,*]

[a] State Key Laboratory of Bioreactor Engineering, East China University of Science and Technology, Shanghai 200237, China
[b] Department of Biotechnology, College of Life Sciences, Ritsumeikan University, Kusatsu 525-8577, Japan

HIGHLIGHTS

- ^{13}C-based metabolic flux analysis was performed for oleaginous yeast *T. cutaneum*.
- Central metabolic network model of *T. cutaneum* was constructed.
- Reaction catalyzed by cytoplasmic malic enzyme was the major source of NADPH.
- Citrate pyruvate cycle played an essential role for lipid accumulation.
- Provide metabolic engineering strategies to biodiesel production.

ARTICLE INFO

Article history:
Received 22 October 2012
Received in revised form 6 December 2012
Accepted 10 December 2012
Available online 20 December 2012

Keywords:
Metabolic flux analysis
Trichosporon cutaneum
Biodiesel
Malic enzyme
Citrate pyruvate cycle

ABSTRACT

Microbial fermentation for producing biodiesel from lignocellulosic hydrolysates is receiving increasing attention and attempts have been made to screen an oleaginous *Trichosporon* sp. with high lipid content and a strong tolerance to lignocellulose hydrolysates. In order to better understand mechanisms related to its lipid accumulation, metabolic flux analysis was performed under 5 g L^{-1} ammonium sulfate (high nitrogen) and/or 0.4 g L^{-1} ammonium sulfate (low nitrogen) conditions. Cell growth phase and lipid accumulation phase were shown for cells grown under low nitrogen condition. Results of flux distribution demonstrated that NADPH provided by cytosolic malic enzyme and the acetyl-CoA from cytoplasmic citrate by the ATP: citrate lyase were the two primary sources for excess lipid accumulation. Flux data also supported the fact that the citrate pyruvate cycle plays an essential role in the lipid accumulation. The flux information obtained could also motivate new design strategies for oleaginous yeasts for enhanced biodiesel production.

1. Introduction

Diminishing petroleum reserves and the rapid accumulation of greenhouse gases have prompted an interest in the development of transportation fuels from renewable sources. By now, two types of biofuels are commercially available—bioethanol fermented from corn or sugarcane, and diesel esterified from vegetable oils or animal fats. However, productions of these fuels would be competing with world food supply and bring many economic problems and environmental burdens (Somerville et al., 2010). So, the development of new types of renewable fuel should be competing needed. Advanced biofuels could be produced from non-food biomass, such as wheat straw, forest waste and energy crops, and these feedstocks are low cost agricultural byproducts or easily large-scale cultivated, fast-growing and environmentally friendly crops (Zhang et al., 2011). Biodiesel, including fatty acid methyl esters (FAMEs), fatty acid ethyl esters (FAEEs), fatty acid propyl esters (FAPEs), with low water solubility, high-energy density, and low toxicity to the production hosts, is now used in diesel engines at more than two billion gallons per year (Zhang et al., 2011).

Almost all microbes are intrinsically capable of synthesizing fatty acids as precursors of cell essential components and the synthesis rate is very fast. Fatty acids are central hydrocarbon intermediates in the biosynthesis of biodiesel, so microbial fermentation for producing biodiesel from lignocellulosic

Abbreviations: G6P, glucose-6-phosphate; 6PG, 6-phosphogluconate; R5P, pentose-phosphates; F6P, fructose-6-phosphate; E4P, erythrose-4-phosphate; S7P, seduheptulose-7-phosphate; T3P, triose-3-phosphate; 3PG, 3-phoshoglycetate; PEP, phosphoenolpyruvate; PYR, pyruvate; ACA, acetaldehyde; ACE, acetate; AcCoA, acetyl-CoA; OAA, oxaloacetate; CIT, citrate; ICT, isocitrate; AKG, α-ketoglutarate; SUC, succinate; MAL, malate.

* Corresponding author. Tel./fax: +86 21 64250972.
E-mail address: qhua@ecust.edu.cn (Q. Hua).

0960-8524/$ - see front matter © 2012 Elsevier Ltd. All rights reserved.
http://dx.doi.org/10.1016/j.biortech.2012.12.072

hydrolysates would be very promising in the future (Röttig et al., 2010). Furthermore, fatty acid biosynthesis and regulation have been extensively characterized (Chan and Vogel, 2010; Fujita et al., 2007), providing rich information for metabolic engineering of microbial strains. Up to now, researches on the production of biodiesel from microbial fermentation mainly focused on two aspects. One method is to make use of industrial useful microorganisms for biofuel production, such as *Eshcherichia coli* (Liu and Khosla, 2010) and *Saccharomyces cerevisiae* because of their fast growth, simple culture demands and clear genetic background. Overproduction of fatty acids in *E. coli* met with success. Liu et al. (2010) constructed an engineered *E. coli* that could produce 4.5 g L^{-1} day^{-1} fatty acids in a minimal medium, with a carbon molar yield of 20% of the theoretical maximum. An alternative approach is using the native, isolated strains. These strains possess the ability to degrade lignocellulosic materials, resist inhibition by substrates and produce biofuels with high content. Oleaginous yeasts, the isolated native microorganism, can accumulate intracellular lipid in excess of 20% of its dry cell weight, and in some cases up to and even in excess of 70% (Gong et al., 2012; Jin et al., 2012; Wu et al., 2011). However, until now, researches on the oleaginous yeasts focused mainly on the screening of superior strains, and the improvement of the lipid content by optimizing the fermentation conditions (Cheirsilp et al., 2011; Saenge et al., 2011). A systems-level analysis and understanding of the mechanisms underlying lipid accumulation in oleaginous yeasts is still lacking.

Metabolomics and flux analysis have provided a truly orthologous measurement of the cellular response to stress and manipulation (Matsuoka and Shimizu, 2010; Mukhopadhyay et al., 2008; Usui et al., 2012), thus could be applied to study metabolic regulation mechanism, indicate potential bottlenecks, and provide guidance for further improvement. Xiong et al. (2010) performed ^{13}C-labeling experiments and analysis of oleaginous microalga *Chlorella protothecoides*, which therefore directed the metabolic engineering strategies for the improvement of desirable bioproducts.

An oleaginous yeast *Trichosporon cutaneum* 2.1374 with high lipid content and a strong tolerance to lignocellulose degradation compounds was screened previously (Chen et al., 2008). In order to systematically understand the mechanisms underlying lipid accumulation in this strain, metabolic analysis based on the quantification of intracellular metabolic fluxes was performed. This study shows the first time that stable isotope-based intracellular flux quantification can be used to better elucidate and understand mechanisms involved in lipid metabolism in oleaginous yeasts.

2. Methods

2.1. Strain and culture conditions

T. cutaneum 2.1374 was screened in our previous study. The strain was used to investigate the intracellular distribution of carbon fluxes under 5 g L^{-1} ammonium sulfate (high nitrogen) and/or 0.4 g L^{-1} ammonium sulfate (low nitrogen) conditions. The medium composition with high nitrogen content was (per liter): 12 g of glucose, 5.0 g of $(NH_4)_2SO_4$, 3.0 g of KH_2PO_4, 0.5 g of $MgSO_4{\cdot}7H_2O$, 30 mg of L-histidine, 125 mg of L-leucine, 25 mg L^{-1} L-methionine, 40 mg of uracil, 1 mL of a trace element solution, and 1 mL vitamin solution. The trace element solution contains (per liter): 15 g of EDTA, 4.5 g of $ZnSO_4{\cdot}7H_2O$, 0.3 g of $CoCl_2{\cdot}6H_2O$, 1.0 g of $MnCl_2{\cdot}4H_2O$, 0.3 g of $CuSO_4{\cdot}5H_2O$, 4.5 g of $CaCl_2{\cdot}2H_2O$, 3.0 g of $FeSO_4{\cdot}7H_2O$, 0.4 g of $NaMoO_4{\cdot}2H_2O$, 1.0 g of H_3BO_3, 0.1 g of KI. The vitamin solution contains (per liter): 0.05 g of D-biotin, 1.0 g of calcium pantothenate, 1.0 g of nicotinic acid, 1.0 g of thiamine hydrochloride, 1.0 g of pyridoxine hydrochloride, 0.2 g of para-aminobenzonic acid, 25 g of (myo)inositol. For the medium with low nitrogen content, $(NH_4)_2SO_4$ concentration was reduced to 0.4 g L^{-1}, and all other components were kept unchanged.

Strains were inoculated into 100 mL medium and cultured overnight at 30 °C. These seed cultures were in turn used to inoculate a 1.5 L fermentor (Shanghai Guoqiang Bioengineering Equipment Co., Shanghai, China) with a working volume of 800 mL. The fermentation temperature was controlled at 30 °C, and the flow rate of air was maintained at 1.5 vvm. Dissolved oxygen (DO), pH and off gas were on-line collected by using the software Biostar.

A mixture of 20% (wt/wt) uniformly ^{13}C-labeled ([U-^{13}C], >99% ^{13}C, Isotec Inc., Miamisburg, OH) and 80% (wt/wt) [1-^{13}C]-labeled glucose (>99%, Cambridge Isotope Laboratories, Andover, MA) was used for all labeling experiments. Each culture was inoculated from a preculture with a starting optical density at 600 nm (OD_{600}) of less than 0.01.

2.2. Determination of physiological parameters

Cell growth during cultivation was monitored at OD_{600}. Dry cell weight (DCW) was determined from cell pellets of 100 mL culture aliquots that were centrifuged for 10 min at 4 °C and 8000*g*, washed once with distilled water, and dried at 85 °C until the weight was constant. The cell density corresponded to OD_{600} value by a regression equation: $y = 0.2731x$ ($R^2 = 0.992$), where x is the absorbance of the suspension at 600 nm, y is the cell density (g DCW L^{-1}). Carbon content of the dried biomass was then determined using an elemental analyzer (Elementar Vario EL III, Germany).

For extracellular metabolite analysis, culture samples were centrifuged for 5 min at 4 °C and 20,000*g* to remove the cells. The depletion of glucose and the secretion of glycerol were determined using commercial enzymatic assay kits. The consumption of ammonia was determined by the method of Weatherburn (1967). The secretion of succinate, acetate, lactate, ethanol and other metabolites in the medium were detected by high-pressure liquid chromatography (SHIMADZU HPLC, Kyoto, Japan). The emissions of carbon dioxide were detected by an exhaust mass spectrometer (MAX300-LG, Extrel CMS, LLC, Pittsburgh, PA).

Based on the correlation factor for dry cell weight and the above concentration change data, physiological parameters of biomass yield ($Y_{X/S}$), specific growth rate (μ), product yield ($Y_{P/S}$), specific glucose uptake rate (q_S), specific product secretion rate (q_P), carbon dioxide evolution rate (CER) and the distribution of carbon in fermentor were determined for the exponentially growing cells (Sauer et al., 1999).

The protein content was determined using Bradford method (Bradford, 1976). The composition and contents of lipids were measured by GC–MS described below. Carbohydrate was measured using the Phenol–sulfuric acid method (Herbert et al., 1971). The KOH/UV method (Benthin et al., 1991) and modified Schneider method (Herbert et al., 1971) was employed for the determination of RNA and DNA, respectively.

2.3. Lipid analysis

The method to determine total lipid weight was similar to that described in Bligh and Dyer (1959) with minor modifications. Cell pellets of 100 mL culture aliquots were centrifuged for 10 min at 4 °C and 8000*g*, washed once with distilled water to remove the extracellular fat from the cell surface and superfluous nutrient substances and then disrupted and homogenized in 6 mL of 4 mol L^{-1} hydrochloric acid for 30 min. The cell debris were mixed well and incubated at 100 °C for 10 min, and then quenched at −20 °C. Frozen cell debris were stirred with 20 mL methanol–chloroform mix-

ture (methanol–chloroform = 1:2 by the volume ratio) for 30 min. After centrifuged for 10 min at 8000*g*, the chloroform layer containing all the lipids was isolated, and the solvent was removed by evaporation. The total lipid was measured by the gravimetric method.

The lipid composition was analyzed by GC–MS. Dissolved the extracted lipid in 3 mL 0.5 mol L^{-1} potassium hydroxide–methanol solution, and let stand in the 90 °C water for 30 min. Then added 3 mL of 14% boron trifluoride methanol solution, and reacted in 75 °C water for 20 min. After the reaction, 1 mL saturated sodium chloride solution was added. After centrifugation, the supernatant was dried under nitrogen, and then dissolved in a certain volume of hexane. After filtration, 0.2 μL of derivatized sample was injected into the Agilent 6890-5975 (GC–MS) (Agilent Technologies, Santa Clara, CA). The HP-5 ms column (30 m × 0.25 mm × 0.25 μm) (Agilent Technologies) was used for GC–MS analysis. GC oven temperature was programmed from 180 °C (2 min) to 250 °C at 5 °C/min, and flow rate of carrier gas was set at 1 mL/min. Other settings were as follows: 250 °C of interface temperature, 230 of ion source temperature, and electron impact ionization (EI) at −70 eV with a full scan ranging from 70 to 560 *m/z* and a solvent delay of 1.5 min.

2.4. Proteinogenic amino acids preparation and GC–MS analysis

The subsequent preparation of proteinogenic amino acid samples for GC–MS analysis was similar to that described elsewhere (Hua et al., 2006) with minor modifications. The cell pellet was washed once with 1 mL distilled water and then hydrolyzed in 200 μL of 6 mol L^{-1} HCl at 105 °C for 16 h. The hydroysate was dried in a heating block at 60 °C for about 8 h and the proteinogenic amino acids were derivatized at 85 °C for 1 h in 100 μL N,N-dimethylformamide and 50 μL N-methyl-N-[tert-butyldimethylsilyl] trifluoroacetamide (Sigma–Aldrich, Saint Louis, MO). After filtration, the derivatized samples were analyzed by GC–MS (Liu et al., 2012).

2.5. In vitro enzymatic assay

In vitro enzyme activities were analyzed in crude cell extracts from 10 mL culture aliquots that were centrifuged at 4 °C and 12,000*g* for 5 min. The cell pellets were washed twice with disruption buffer that contained 200 mmol L^{-1} Tris–HCl (pH 7.6), 4 mmol L^{-1} $MgCl_2$, and 2 mmol L^{-1} dithiothreitol, and the cell pellets were then ground in the presence of liquid nitrogen. The protein concentration of cell extracts was determined using Bradford method (Bradford, 1976). The activity of malic enzyme was assayed by monitoring the increase in absorbance of NADPH.

2.6. Metabolic modeling and flux analysis

For metabolic flux ratio analysis, a mass isotopomer distribution vector of each amino-acid fragment MDV_α (Eq. (1)) was assigned based on the well-developed mathematic methodology (Nanchen et al., 2007).

$$MDV_\alpha = \begin{bmatrix} (m_0) \\ (m_1) \\ \vdots \\ (m_n) \end{bmatrix} \quad \text{with} \quad \sum_{i=0}^{n} m_i = 1 \tag{1}$$

Where m_0 is the fractional abundance of fragments with monoisotopic mass and $m_{i>0}$ the abundance of molecules with higher masses.

To obtain the exclusive mass isotope distribution of the carbon skeleton MDV^*_α, MDV_α were corrected for the natural isotope abundance of H, O, N, S, Si, and C atoms in the derivatized groups and for the natural isotope abundance of H, O, N, S atoms in the amino acid using a correction matrix (Eq. (2)) as described by Nanchen et al. (2007).

$$MDV^*_\alpha = {C_{corr,CHONSSi}}^{-1} \cdot MDV_\alpha \tag{2}$$

The correction matrix $C_{corr,CHONSSi}$ was obtained from the correction matrices for all individual atom species (Eq. (3)).

$$C_{corr,CHONSSi} = C_{corr,C} \cdot C_{corr,H} \cdot C_{corr,O} \cdot C_{corr,N} \cdot C_{corr,S} \cdot C_{corr,Si} \tag{3}$$

And then the contribution of ^{13}C from the unlabeled biomass in culture inocula was subtracted from MDV^*_α, yielding mass distribution vector of amino acid MDV_{AA} according to Eq. (4).

$$MDV_{AA} = \frac{MDV^*_\alpha - f_{unlabeled} \cdot MDV_{unlabeled,n}}{1 - f_{unlabeled}} \tag{4}$$

where $f_{unlabeled}$ is the fraction of the unlabeled biomass, which was caused by inoculation and $MDV_{unlabeled,n}$ is the mass distribution of an unlabeled fragment with n C atoms.

3. Results and discussion

3.1. Influence of nitrogen concentration on growth of T. cutaneum 2.1374

T. cutaneum 2.1374 was incubated in 1.5 L fermentor under high and/or low nitrogen condition. The elemental compositions of the dried biomass were determined by an elemental analyzer. The carbon content was 45.3%, which was therefore used in the subsequent analysis of intracellular carbon flow distribution. Typical culture profiles and physiological parameters of the strain under two different nitrogen conditions were shown in Fig. 1 and Table 1. When nitrogen content was relatively high, the cells growth rate was high but the growth ceased at about 24 h. In comparison, the cell growth could last for around 60 h with low nitrogen concentration in the medium, albeit at low growth rate (Fig. 1A and B). Correspondingly, the depletion of glucose in the high nitrogen medium was significantly faster than that in the medium with less nitrogen content (Fig. 1C). The residual NH_4^+ concentration was about 41 mmol L^{-1} under high nitrogen condition, while no residual NH_4^+ was detected in the nitrogen-limited medium (Fig. 1D). Only a small amount of ethanol was secreted by the strain under high nitrogen condition (Fig. 1D).

Nitrogen limitation resulted in a decrease in cell growth rate, glucose uptake rate, NH_4^+ uptake rate and carbon dioxide evolution rate (CER), but an increase in biomass yield. Compared to a biomass yield of approximately 0.64 g DCW/g glucose under high nitrogen condition, about 15% increase was obtained by cells grown with nitrogen limitation. Fig. 2 shows the distribution of carbon in cells under two different conditions. Glucose carbon flow was mainly directed towards biomass under both nitrogen conditions, where the conversion to biomass was more efficient in case the supply of nitrogen was limited. It should however be noted that dissolved oxygen was not controlled in this study. In addition to nitrogen concentration, DO concentration in the medium might also affect the cell growth as well as lipid production to some extent, which should therefore be taken into consideration in future studies for more reliable analysis.

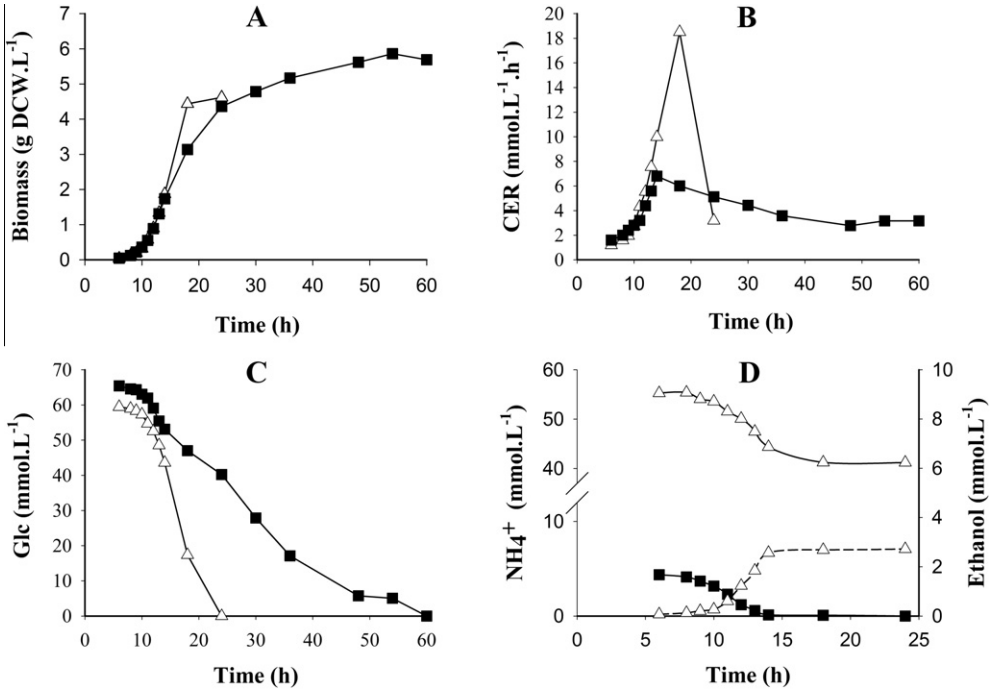

Fig. 1. Aerobic batch cultivation of *T. cutaneum* 2.1374 under different nitrogen concentration conditions. (A) biomass concentration; (B) carbon dioxide evolution rate (CER); (C) glucose concentration; and (D) NH_4^+ (nitrogen) and ethanol concentrations, the dashed line indicates ethanol secretion under high nitrogen condition. Symbols, △: high nitrogen condition; ■: low nitrogen condition.

Table 1
Growth parameters for *T. cutaneum* 2.1374 under different nitrogen conditions.

	μ_{max} (h^{-1})	$q_{NH_4^+}$ (mmol g^{-1} h^{-1})	q_{Glc} (mmol g^{-1} h^{-1})	q_{Eth} (mmol g^{-1} h^{-1})	$q_{Biomass}$ (mmol g^{-1} h^{-1})	q_{CO_2} (mmol g^{-1} h^{-1})	$Y_{X/S}$ (g g^{-1})	*C* balance (%)
High N	0.48 ± 0.01	2.91 ± 0.01	4.18 ± 0.02	0.68 ± 0.04	18.24 ± 0.03	4.80 ± 0.04	0.64 ± 0.04	97.3
Low N	0.46 ± 0.01	1.76 ± 0.01	3.43 ± 0.02	0	17.26 ± 0.03	3.01 ± 0.04	0.74 ± 0.04	98.6

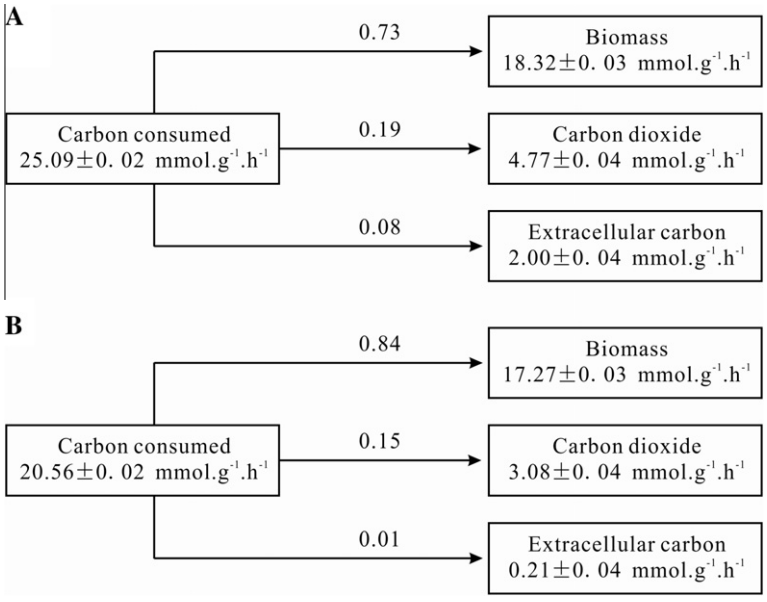

Fig. 2. Distribution of carbon in *T. cutaneum* under high nitrogen condition (A) and low nitrogen condition (B).

Table 2
Macromolecular compositions of *T. cutaneum* 2.1374 (g/g DCW).

	Lipid (%)	Protein (%)	Carbohydrate (%)	DNA (%)	RNA (%)	Others (%)
High *N*	8.3 ± 0.2	48.5 ± 0.3	30.2 ± 0.4	0.4 ± 0.2	3.9 ± 0.3	8.7 ± 0.4
Low *N*	31.0 ± 0.2	27.3 ± 0.3	31.2 ± 0.4	0.4 ± 0.2	4.0 ± 0.3	6.1 ± 0.4

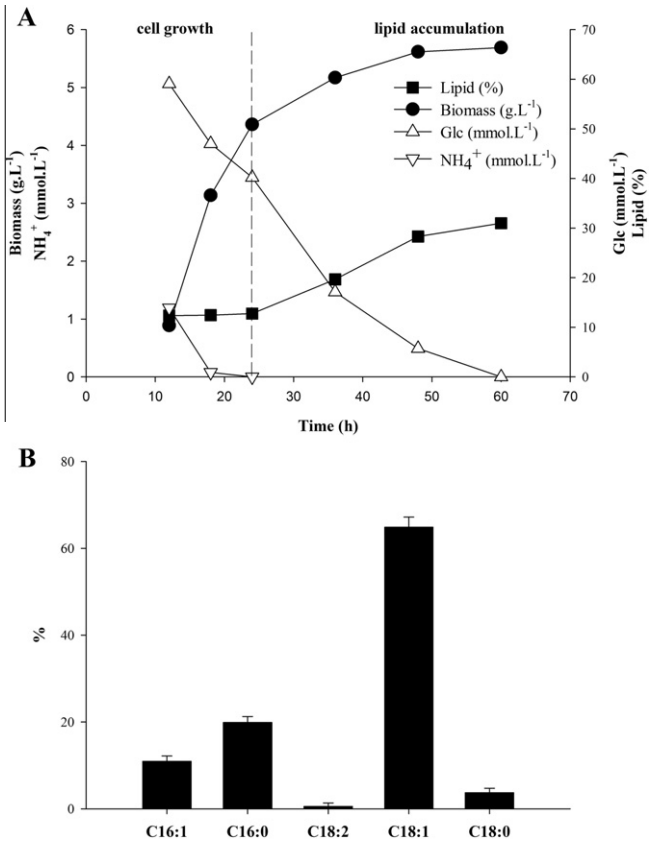

Fig. 3. (A) Profiles of cell growth and lipid accumulation under limited nitrogen condition; and (B) typical lipid composition of *T. cutaneum* 2.1374 under limited nitrogen condition.

3.2. Influence of nitrogen concentration on lipid accumulation of T. cutaneum 2.1374

In order to elucidate the influence of nitrogen concentration on macromolecular compositions of *T. cutaneum* 2.1374, contents of five major cell components (carbohydrate, lipid, protein, DNA and RNA) that accounted for 85% of total dry cell weight, were analyzed and listed in Table 2. No significant effects were observed on carbohydrate, DNA and RNA by nitrogen in the medium. The contents of lipid and protein, however, changed dramatically between two culture conditions. With the marked decrease in nitrogen concentration, the lipid content increased sharply from 8.3% to about 31%, whereas the protein content in nitrogen-deprived cells dropped greatly from 48.5% to 27.3%.

The profiles of lipid accumulation and biomass synthesis under nitrogen limitation were depicted in Fig. 3A. The growth of *T. cutaneum* 2.1374 on glucose and limited nitrogen source could be roughly divided into cell growth phase (before 24 h of culture) and lipid accumulation phase (24–60 h). The cells grew very fast before the depletion of nitrogen source, whereas the lipid content remained almost unchanged (less than 15% of dry cell weight), this period can be identified as the cell growth phase. When nitrogen was completely exhausted from the medium (24 h and later), the lipid content increased significantly to its maximum (approximately 31% g/g DCW) at about 60 h, while the cell growth rate declined markedly due to the lack of nitrogen source. These physiological results under nitrogen limitation were therefore in good agreement with those reported elsewhere (Fontanille et al., 2012), i.e. when nitrogen concentration in the medium was extremely low, the glucose assimilated was mainly used for cell maintenance and lipid accumulation instead of cell production. Besides, *T. cutaneum* 2.1374 accumulated storage lipid under nitrogen starvation and probably degraded it to other metabolites under carbon starvation conditions, like other commonly oleaginous microorganisms (Makri et al., 2010). The compositions of lipid accumulated under limited nitrogen condition were assayed, and Fig. 3B shows that the major lipid compositions included oleic acid (C18:1, ca. 65% w/w), palmitic acid (C16:0, ca. 20%) and palmitoleic acid (C16:1, ca. 11%).

3.3. Metabolic network construction for T. cutaneum 2.1374

As shown above, the lipid content of *T. cutaneum* 2.1374 reached about 31% (g/g DCW) under low nitrogen condition, and the metabolism was divided into cell growth phase and lipid accumulation phase. In order to understand the mechanisms underlying the lipid accumulation and suggest further modifications for the improvement of lipid synthesis, ratios of metabolic fluxes at several key metabolic nodes were analyzed based on ^{13}C-labeling experiments as well as enzymatic activity analysis for the strain grown under low nitrogen condition. Cell samples were taken at mid-logarithmic growth phase (around 12 h) and lipid accumulation phase (around 42 h) for labeling analysis of intracellular flux ratios.

Bioreaction network of the central carbon metabolism of *T. cutaneum* 2.1374 is required for the flux analysis. Previous studies revealed that mitochondrial citrate in oleaginous yeast cells accumulates in response to the depletion of nitrogen in the medium, and the excessive citrate in mitochondrion is then transported into the cytosol. ATP-citrate lyase (ACL), existing within the cytoplasm of oleaginous yeasts, is responsible for of the cleavage of citrate to acetyl-CoA and oxaloacetate (Meng et al., 2009; Ratledge and Wynn, 2002). The above-mentioned information, together with the knowledge of yeast metabolic characteristics (Blank et al., 2005; Blank and Sauer, 2004), was therefore applied to the construction of the metabolic network of *T. cutaneum* 2.1374 (Fig. 4 and Appendix). The metabolic properties and relative metabolic flux distributions of nitrogen-limited cells were then studied based on the constructed network models with the pentose phosphate (PP) pathway, the tricarboxylic acid (TCA) cycle, the glycolytic pathway (EMP), the citrate pyruvate cycle, and reactions via malic enzyme.

3.4. Mechanisms of lipid accumulation in T. cutaneum 2.1374

In this study, metabolic flux ratio analysis, which has proven to be a useful tool to characterize many organisms and reveal biologically important mechanisms, was performed to better elucidate

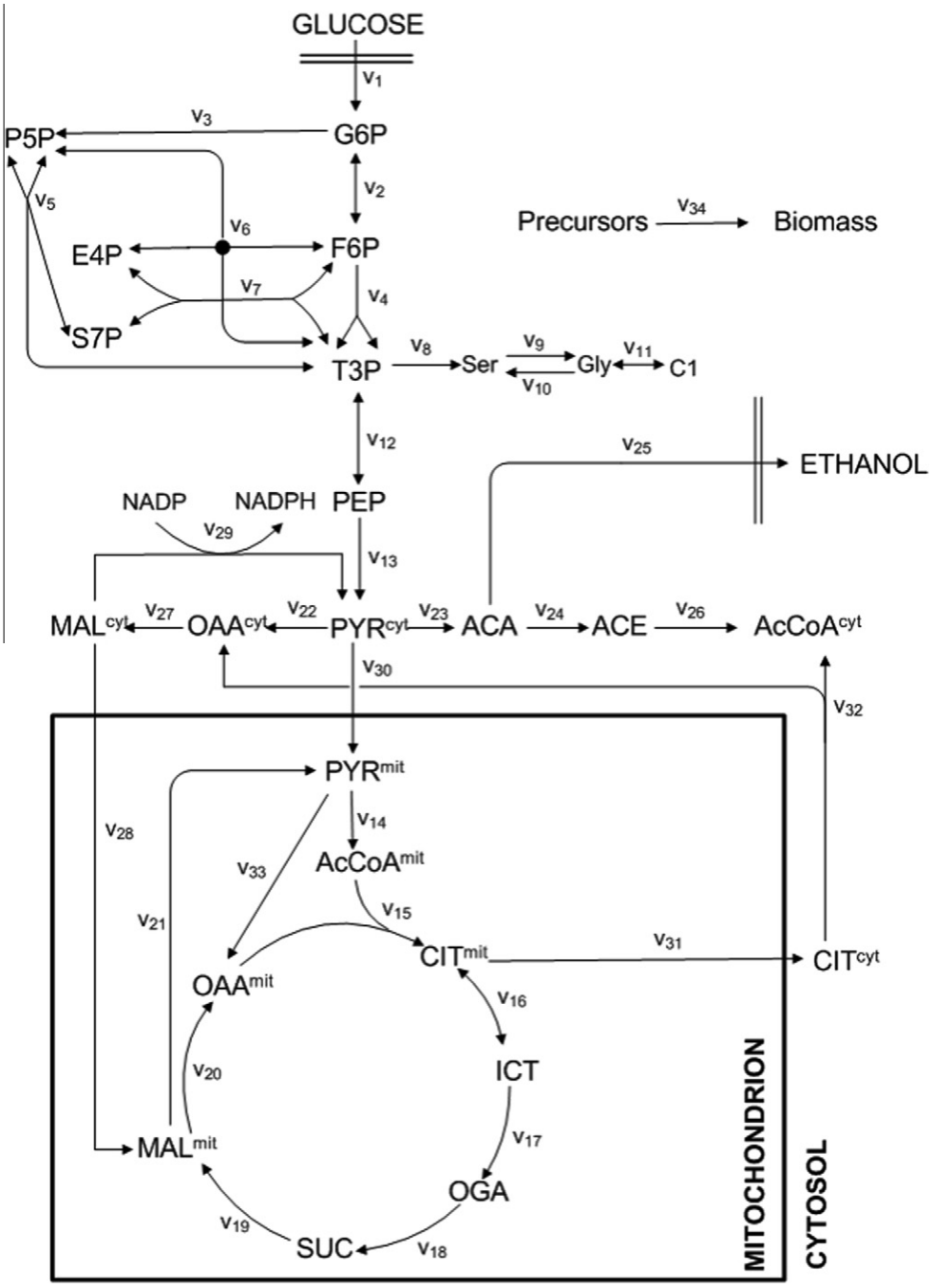

Fig. 4. Bioreaction network of *T. cutaneum* 2.1374 central carbon metabolism.

and understand mechanisms related to lipid accumulation in *T. cutaneum* 2.1374 under nitrogen limitation. Several flux ratios, including OAA originating from PYR in cytoplasm, mitochondrial OAA from anaplerosis by the carboxylation of mitochondrial pyruvate, PEP from glycolysis in cytoplasm, and PYR originating from MAL in mitochondrion.

By comparing ^{13}C isotopomer distribution data of the target metabolites with those of the source metabolites originating from individual pathways, metabolic flux ratios at several key metabolic nodes were quantified and detailed in Fig. 5A. Increases in the fraction of the mitochondrial OAA originating from anaplerosis by the carboxylation of mitochondrial pyruvate and the fraction of PYR originating from mitochondrial MAL were observed in lipid accumulation phase compared to those obtained for exponentially growing cells. The fraction of OAA originating from PYR in cytoplasm was found lower in the lipid accumulation phase, and no significant difference was observed for the contribution of glycolysis to glucose catabolism under two metabolic phases, as shown by the ratio of PEP from glycolysis in Fig. 5A.

High content of lipid accumulated in oleaginous microorganisms requires the supply of a large amount of acetyl-CoA as the precursor and reducing equivalent (NADPH) as the cofactor for

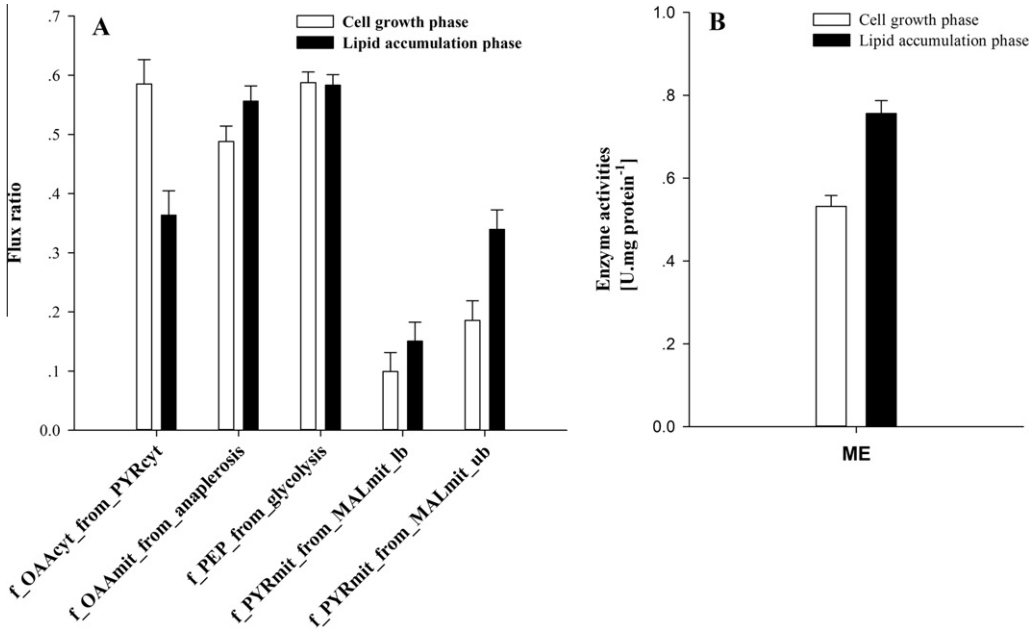

Fig. 5. Flux ratios (A) and activities of cytoplasmic malic enzyme (B) in both cell growth and lipid accumulation phases of *T. cutaneum* 2.1374 under limited nitrogen condition.

fatty acid synthesis. Generally, NADPH for fatty acid biosynthesis is mainly generated from pentose phosphate pathway and $NADP^+$ dependent malic enzyme in microorganisms. In oleaginous yeasts, $NADP^+$ dependent malic enzyme is located in cytoplasm and was known to play a key role in lipid accumulation (Botham and Ratledge, 1979; Holdsworth et al., 1988; Ratledge and Wynn, 2002). Our results showed that the flux distributions between the pentose phosphate pathway and the glycolytic pathway remained almost unchanged in both cell growth and lipid accumulation phases, whereas the activity of cytoplasmic malic enzyme was detected to be higher in lipid accumulation phase compared to that in cell growth phase (Fig. 5B). The data obtained in this study therefore suggested that the reaction via the cytoplasmic malic enzyme (reaction 29 in Fig. 4) was the primary source of reducing equivalent for lipid accumulation in *T. cutaneum* 2.1374, which was also in good agreement with the results published elsewhere.

Cytoplasmic OAA could be derived from two pools: (i) cytoplasmic PYR (ii) cytoplasmic citrate by ATP-citrate lyase. The results in Fig. 5A showed a significantly lowered fraction of OAA originating from cytoplasmic PYR in lipid accumulation phase, indicating an increase in activity of ATP-citrate lyase (reaction 32 in Fig. 4) when nitrogen in the medium was depleted.

Pyruvate cycling may occur via the "citrate pyruvate cycle" involving pyruvate carboxylase-catalyzed conversion of pyruvate to oxaloacetate. Oxaloacetate was then converted to citrate, which was transported outside the mitochondria and degradated into OAA and AcCoA in the cytoplasm. Malate obtained from OAA could then be decarboxylated to generate pyruvate either via the NADP-dependent cytosolic malic enzyme or via NAD-dependent mitochondrial malic enzyme (Ronnebaum et al., 2006). The fraction of the mitochondrial OAA originating from anaplerosis by the carboxylation of mitochondrial pyruvate was increased in lipid accumulation phase. In addition, the fraction of PYR originating from MAL via the NAD-dependent mitochondrial malic enzyme was also increased in lipid accumulation phase. These results showed that the first and the last step of the citrate pyruvate cycle were both enhanced during lipid accumulation. Therefore, based on the quantification of metabolic flux contributions, the citrate pyruvate cycle was also found to play an essential role in generating cytosolic acetyl-CoA for lipid biosynthesis in *T. cutaneum*.

4. Conclusions

Compared with the growth of *T. cutaneum* 2.1374 with sufficient nitrogen supply, biomass yield of cells was increased and the lipid content reached approximately 31% (g/g DCW) in case that nitrogen concentration in the medium was limited. Based on the growth and metabolic characteristics studied for this oleaginous yeast, the reaction via cytoplasmic $NADP^+$-dependent malic enzyme was confirmed to be the major source of reducing equivalent for the lipid accumulation in *T. cutaneum*. Intracellular flux information also showed a significant effect of the citrate pyruvate cycle on lipid biosynthesis by providing adequate cytoplasmic acetyl-CoA. These flux-based results might motivate new metabolic design and engineering of above-mentioned two pathways to enhance the biodiesel production with this strain or related oleaginous yeasts.

Acknowledgements

This work was financially supported by National Basic Research Program of China (973 Program) (2012CB721101), Fundamental Research Funds for the Central Universities of China (WF0913005), Research Fund for the Doctoral Program of Higher Education of China (20110074110014), and partly supported by National Special Fund for State Key Laboratory of Bioreactor Engineering (2060204), and Shanghai Leading Academic Discipline Project (B505). The authors are grateful to the help provided by Professor Siliang Zhang in fermentation and Li Zhou in GC–MS analysis.

Appendix A

The central metabolic network in T. cutaneum 2.1374 with the stoichiometric reactions

Reactions	
v1	Glucose + ATP > G6P
v2	G6P = F6P
v3	G6P + 2 ∗ NADP > P5P + 2 ∗ NADPH + CO2
v4	F6P + ATP > 2 ∗ T3P + ADP + Pi
v5	2 ∗ P5P = S7P + T3P
v6	P5P + E4P = F6P + T3P
v7	S7P + T3P = E4P + F6P
v8	T3P + NAD > SER + NADH
v9	SER + NADH > GLY + C1 + NAD
v10	GLY + NAD + C1 > SER + NADH
v11	C1 + CO2 + NADH = GLY + NAD
v12	T3P + NAD = PEP + ATP + NADH
v13	PEP + ADP + Pi > cyt PYR + ATP
v14	mit PYR + NAD > mit AcCoA + CO_2 + NADH
v15	mit OAA + mit AcCoA > mit CIT
v16	mit CIT = ICT
v17	ICT+ NAD > OGA+ CO2 + NADH
v18	OGA + NAD > SUC+ CO2 + NADH
v19	SUC > mit MAL
v20	mit MAL > mit OAA
v21	mit MAL + NAD > mit PYR + CO2 + NADH
v22	cyt PYR + CO2 + ATP > cyt OAA + ADP + Pi
v23	cyt PYR > ACA + CO2
v24	ACA + NADP = ACE + NADPH
v25	ACA + NADH = ethanol
v26	ACE + 2 ∗ ATP > cyt AcCoA + 2 ∗ ADP + 2 ∗ Pis
v27	OAA > cytMAL
v28	cyt MAL > mit MAL
v29	cyt MAL + NADP > cyt PYR + CO2 + NADPH
v30	cyt PYR > mPYR
v31	mit CIT > cyt CIT
v32	cyt CIT > cyt AcCoA + cyt OAA
v33	mit PYR + ATP + CO2 > mit OAA + ADP + Pi
v34	Precursors > biomass

Note: mit, mitochondrial; cyt, cytoplasmic.

References

Benthin, S., Nielsen, J., Villadsen, J., 1991. A simple and reliable method for the determination of cellular RNA content. Biotechnol. Tech. 5, 39–42.

Blank, L.M., Kuepfer, L., Sauer, U., 2005. Large-scale ^{13}C-flux analysis reveals mechanistic principles of metabolic network robustness to null mutations in yeast. Genome Biol. 6, R49.1–R49.16.

Blank, L.M., Sauer, U., 2004. TCA cycle activity in *Saccharomyces cerevisiae* is a function of the environmentally determined specific growth and glucose uptake rates. Microbiology 150, 1085–1093.

Bligh, E.G., Dyer, W.J., 1959. A rapid method of total lipid extraction and purification. Can. J. Biochem. Phys. 37, 911–917.

Botham, P.A., Ratledge, C., 1979. A biochemical explanation for lipid accumulation in *Candida* 107 and other oleaginous micro-organisms. J. Gen. Microbiol. 114, 361–375.

Bradford, M., 1976. A rapid and sensitive method for the quantitation of microgram quantities of protein utilizing the principle of protein–dye binding. Anal. Biochem. 72, 248–254.

Chan, D., Vogel, H., 2010. Current understanding of fatty acid biosynthesis and the acyl carrier protein. Biochem. J. 430, 1–19.

Cheirsilp, B., Suwannarat, W., Niyomdecha, R., 2011. Mixed culture of oleaginous yeast *Rhodotorula glutinis* and microalga *Chlorella vulgaris* for lipid production from industrial wastes and its use as biodiesel feedstock. New Biotechnol. 28, 362–368.

Chen, X., Li, Z., Zhang, X., Hu, F., Ryu, D., Bao, J., 2008. Screening of oleaginous yeast strains tolerant to lignocellulose degradation compounds. Appl. Biochem. Biotechnol., 1–14.

Fontanille, P., Kumar, V., Christophe, G., Nouaille, R., Larroche, C., 2012. Bioconversion of volatile fatty acids into lipids by theoleaginous yeast *Yarrowia lipolytica*. Bioresour. Technol. 114, 443–439.

Fujita, Y., Matsuoka, H., Hirooka, K., 2007. Regulation of fatty acid metabolism in bacteria. Mol. Microbiol. 66, 829–839.

Gong, Z., Wang, Q., Shen, H., Hu, C., Jin, G., Zhao, Z.K., 2012. Co-fermentation of cellobiose and xylose by *Lipomyces starkeyi* for lipid production. Bioresource Technol. 117, 20–24.

Herbert, D., Phipps, P., Strange, R., 1971. Chapter III chemical analysis of microbial cells. Methods Microbiol. 5, 209–344.

Holdsworth, J.E., Veenhuis, M., Ratledge, C., 1988. Enzyme activities in oleaginous yeasts accumulating and utilizing exogenous or endogenous lipids. J. Gen. Microbiol. 134, 2907–2915.

Hua, Q., Joyce, A.R., Fong, S.S., Palsson, B.O., 2006. Metabolic analysis of adaptive evolution for in silico-designed lactate-producing strains. Biotechnol. Bioeng. 95, 992–1002.

Jin, G., Yang, F., Hu, C., Shen, H., Zhao, Z.K., 2012. Enzyme-assisted extraction of lipids directly from the culture of the oleaginous yeast *Rhodosporidium toruloides*. Bioresour. Technol. 111, 378–382.

Liu, T., Khosla, C., 2010. Genetic engineering of *Escherichia coli* for biofuel production. Annu. Rev. Genet. 44, 53–69.

Liu, T., Vora, H., Khosla, C., 2010. Quantitative analysis and engineering of fatty acid biosynthesis in *E. coli*. Metab. Eng. 12, 378–386.

Liu, Z., Wang, X., Qi, Q., Hua, Q., 2012. Quantification and analysis of metabolic characteristics of aerobic succinate-producing *Escherichia coli* under different aeration conditions. Process Biochem. 47, 1532–1538.

Makri, A., Fakas, S., Aggelis, G., 2010. Metabolic activities of biotechnological interest in *Yarrowia lipolytica* grown on glycerol in repeated batch cultures. Bioresour. Technol. 101, 2351–2358.

Matsuoka, Y., Shimizu, K., 2010. Current status of ^{13}C-metabolic flux analysis and future perspectives. Process Biochem. 45, 1873–1881.

Meng, X., Yang, J., Xu, X., Zhang, L., Nie, Q., Xian, M., 2009. Biodiesel production from oleaginous microorganisms. Renew. Energ. 34, 1–5.

Mukhopadhyay, A., Redding, A.M., Rutherford, B.J., Keasling, J.D., 2008. Importance of systems biology in engineering microbes for biofuel production. Curr. Opin. Biotech. 19, 228–234.

Nanchen, A., Fuhrer, T., Sauer, U., 2007. Determination of metabolic flux ratios from ^{13}C-experiments and gas chromatography–mass spectrometry data: protocol and principles. Methods Mol. Biol. 358, 177–197.

Röttig, A., Wenning, L., Bröker, D., Steinbüchel, A., 2010. Fatty acid alkyl esters: perspectives for production of alternative biofuels. Appl. Microbiol. Biotechnol. 85, 1713–1733.

Ratledge, C., Wynn, J.P., 2002. The biochemistry and molecular biology of lipid accumulation in oleaginous microorganisms. Adv. Appl. Microbiol. 51, 1–51.

Ronnebaum, S.M., Ilkayeva, O., Burgess, S.C., Joseph, J.W., Lu, D., Stevens, R.D., Becker, T.C., Sherry, A.D., Newgard, C.B., Jensen, M.V., 2006. A pyruvate cycling pathway involving cytosolic NADP-dependent isocitrate dehydrogenase regulates glucose-stimulated insulin secretion. J. Biol. Chem. 281, 30593–30602.

Saenge, C., Cheirsilp, B., Suksaroge, T.T., Bourtoom, T., 2011. Potential use of oleaginous red yeast *Rhodotorula glutinis* for the bioconversion of crude glycerol from biodiesel plant to lipids and carotenoids. Process Biochem. 46, 210–218.

Sauer, U., Lasko, D., Fiaux, J., Hochuli, M., Glaser, R., Szyperski, T., Wuthrich, K., Bailey, J., 1999. Metabolic flux ratio analysis of genetic and environmental modulations of *Escherichia coli* central carbon metabolism. J. Bacteriol. 181, 6679–6688.

Somerville, C., Youngs, H., Taylor, C., Davis, S.C., Long, S.P., 2010. Feedstocks for lignocellulosic biofuels. Science 329, 790–792.

Usui, Y., Hirasawa, T., Furusawa, C., Shirai, T., Yamamoto, N., Mori, H., Shimizu, H., 2012. Investigating the effects of perturbations to *pgi* and *eno* gene expression on central carbon metabolism in *Escherichia coli* using ^{13}C metabolic flux analysis. Microb. Cell Fact. 11, 87.

Weatherburn, M., 1967. Phenol–hypochlorite reaction for determination of ammonia. Anal. Chem. 39, 971–974.

Wu, S., Zhao, X., Shen, H., Wang, Q., Zhao, Z.K., 2011. Microbial lipid production by *Rhodosporidium toruloides* under sulfate-limited conditions. Bioresour. Technol. 102, 1803–1807.

Xiong, W., Liu, L., Wu, C., Yang, C., Wu, Q., 2010. ^{13}C tracer and gas chromatography–mass spectrometry analyses reveal metabolic flux distribution in the oleaginous microalga *Chlorella protothecoides*. Plant Physiol. 154, 1001–1011.

Zhang, F., Rodriguez, S., Keasling, J., 2011. Metabolic engineering of microbial pathways for advanced biofuels production. Curr. Opin. Biotechnol. 22, 1–9.